Journal of Drug Delivery Science and Technology xxx (xxxx) xxxx

Contents lists available at ScienceDirect

Journal of Drug Delivery Science and Technology

journal homepage: www.elsevier.com/locate/jddst

Precise ratiometric co-loading, co-delivery and intracellular co-release of paclitaxel and curcumin by aid of their conjugation to the same gold nanorods to exert synergistic effects on MCF-7/ADR cells

Shaohui Xu[a,1], Zhu Jin[a,1], Zhipeng Zhang[b,1], Wei Huang[c,d], Yuanyuan Shen[a,*], Zhongmin Wang[c,d,**], Shengrong Guo[a,***]

[a] School of Pharmacy, Shanghai Jiao Tong University, Shanghai, 200240, China
[b] School of Pharmacy, Hubei University of Science and Technology, Xianning, 437100, China
[c] Department of Interventional Radiology, Ruijin Hospital, Shanghai Jiao Tong University School of Medicine, Shanghai, 200025, China
[d] Department of Interventional Radiology, Ruijin Hospital Luwan Branch, Shanghai Jiao Tong University School of Medicine, Shanghai, 200020, China

ARTICLE INFO

Keywords:
Gold nanorods
Precise ratiometric
Synergistic effect
Co-release
Co-delivery

ABSTRACT

It is necessary for effective combinational effects that multiple chemotherapeutic agents enter and act on the same tumor cells simultaneously at a suitable ratio. Due to their individual physicochemical or biopharmaceutical properties, they cannot reach the same cells at its predetermined ratio after co-administration. Herein, we report a novel system with precise ratiometric co-loading, co-delivery and intracellular co-release of paclitaxel (PTX) and curcumin (CUR), to investigate their synergistic effects. We prepared the system by conjugating PTX and CUR at different ratios onto the same gold nanorods (GNRs). We demonstrated that PTX and CUR could be precisely ratiometric co-loaded to form dual-drug conjugated biotin-PEG modified GNRs (abbreviated as PTX/CUR@BPGNRs), which could co-deliver dual drugs into tumor cells with a predetermined ratio and co-release them intracellularly. The PTX/CUR@BPGNRs with the mass ratio of PTX and CUR at 1:1 exhibited the best synergistic effect on multidrug resistant MCF-7/ADR cells while the free PTX and CUR mixture with the mass ratio of at 1:0.75 displayed the strongest synergism. Cytotoxicity studies showed that PTX/CUR@BPGNRs are superior to free drug mixture. Furthermore, PTX/CUR@BPGNRs could remarkably induce apoptosis of MCF-7/ADR cells under near-infrared irradiation. Moreover, we found that PTX/CUR@BPGNRs significantly inhibited P-glycoprotein (P-gp) expression in MCF-7/ADR cells.

1. Introduction

Multidrug resistance (MDR) is one of the main causes leading to chemotherapy failure and the overexpression of ATP-dependent drug efflux pumps such as permeability glycoprotein (P-gp) is considered as the primary cause [1,2]. Combination therapy has shown superior antitumor efficiency to reverse MDR due to their different mechanisms of action. As is widely recognized, synergistic effects, additive effects and antagonistic effects may occur among different ratios of drug combinations [3]. Synergistic effects will be achieved only when drug combinations enter tumor cells at an optimal ratio [4,5]. Therefore, it is essential to ensure the drug combinations are at a predetermined ratio when tumor cells are exposed to multiple drugs, therefore the synergistic therapeutic effects will be maximized.

The approaches to loading multiple drugs into a single nanocarrier can be achieved by physical encapsulation, covalent conjugation or a combination of both methods. To precisely control the loading ratio of different drugs, the method of covalent conjugation is more advantageous because physical encapsulation often leads to premature drug release during blood circulation and is unable to maintain the predetermined drug ratio by the time drugs enter tumor cells [6,7].

With the development of nanotechnology, several nano-drug delivery systems (NDDS), such as liposomes and micelles, have provided the possibility to co-deliver multiple therapeutic agents within a single drug delivery vehicle. However, precisely controlling the loading ratio and release characteristics of multiple drugs remain formidable

* Corresponding author.
** Corresponding author. Department of Interventional Radiology, Ruijin Hospital, Shanghai Jiao Tong University School of Medicine, Shanghai, 200025, China.
*** Corresponding author.
E-mail addresses: shenyuanyuan@sjtu.edu.cn (Y. Shen), wzm11896@rjh.com.cn (Z. Wang), srguo@sjtu.edu.cn (S. Guo).
[1] These authors made equal contributions to this work.

https://doi.org/10.1016/j.jddst.2019.101383
Received 14 July 2019; Received in revised form 4 November 2019; Accepted 9 November 2019

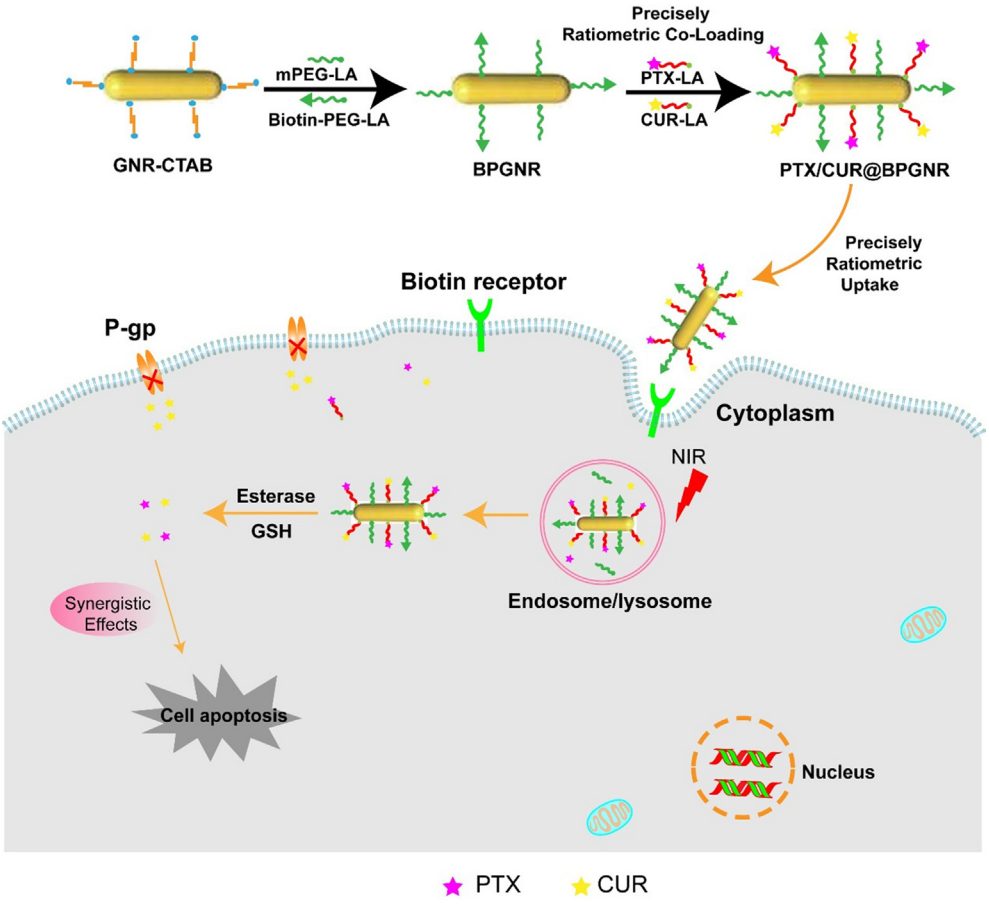

Fig. 1. Schematic illustration of Precise ratiometric co-loading, co-delivery and co-release of PTX and CUR from PTX/CUR@BPGNRs.

challenges [4,8,9]. Functional gold nanomaterials, such as gold nanorods (GNRs) and gold nanocages, have comprehensive applications in the biomedical field, e.g. medical diagnosis, drug delivery and photothermal therapy [10]. Owing to the excellent biocompatibilities, chemical stabilities, unique optical and photothermal properties, gold nanorods have been widely used as platforms for cancer therapy including chemotherapy, photothermal therapy, photodynamic therapy and tumor imaging [11]. GNRs with a longitudinal absorption peak at approximately 808 nm wavelength are frequently used for near-infrared (NIR) triggered drug delivery due to their strong ability to convert NIR irradiation to local heating [12].

Herein, we developed a GNR-based dual-drug conjugation where different drug molecules were conjugated to the same GNRs (Fig. 1). Paclitaxel (PTX) is an anticancer drug widely used in the clinical treatment of breast cancer that induces tubulin polymerization and stabilizes microtubules [13]. Curcumin (CUR), a natural polyphenolic compound, possesses pleiotropic anticancer effects such as inhibiting P-gp expression, NF-κB signaling pathway and angiogenesis [14,15]. Synergistic effects of PTX and CUR have been demonstrated to overcome MDR of PTX in recent studies [16,17]. The covalent bond between gold and sulfur (namely, the Au–S bond) is a robust bond with high binding efficiency that can provide the feasibility to precisely co-load dual-drugs to GNRs [18]. To load drugs onto GNRs, PTX and CUR were first reacted with lipoic acid (LA) to synthesize paclitaxel-lipoic acid ester (PTX-LA) and curcumin-lipoic acid ester (CUR-LA), respectively. To enhance the internalization of GNRs and facilitate effective drug delivery, we modified GNRs with biotin moiety conjugated polyethylene glycol (Biotin-PEG). As reported in many studies, biotin moiety can be specifically bound to biotin receptors, which are overexpressed in various cancer cell lines [19–21]. Next, PTX-LA and CUR-LA at precisely controlled ratios were co-loaded onto the same biotin-PEG-modified GNRs (abbreviated as BPGNRs) via the Au–S bonds to prepare dual-drug loaded GNRs (abbreviated as PTX/CUR@BPGNRs). The two drugs were precisely ratiometrically taken up by MCF-7/ADR cells via biotin receptor-mediated endocytosis. The abundant glutathione (GSH) in the cytoplasm promoted the dissociations of PTX-LA and CUR-LA from GNRs through the ligand exchange reaction of Au–S [22–25]. Additionally, the high-level of esterase in cytoplasm enables ester prodrugs to be quickly hydrolyzed to release free drugs [26–29]. Moreover, the GNRs here absorb and transform NIR irradiation to localized photothermal heating to expedite the hydrolysis of prodrugs [30,31]. Taken together, the same Au–S bond and ester linkage will allow PTX and CUR to be co-released from PTX/CUR@BPGNRs. The therapeutic effects of PTX/CUR@BPGNRs on multidrug-resistant human breast cancer MCF-7/ADR cells were evaluated and the mechanisms of action were investigated. We expect this combinatorial drug delivery system would provide a new paradigm for precise control over drug ratio in combination therapy.

2. Materials and methods

2.1. Materials

Silver nitrate ($AgNO_3$), cetyltrimethylammonium bromide (CTAB), sodium borohydride ($NaBH_4$), 7-Bromo-3-hydroxy-2-naphthoic acid (7-BrHNA), L-ascorbic acid (L-AA), 3-(4,5-dimethylthiazol-2-yl)-2,5-diphenyltetrazolium bromide (MTT), curcumin (CUR), Porcine liver esterase (PLE) and dimethyl sulfoxide (DMSO) were purchased from Sigma-Aldrich (USA). Chloroauric acid ($HAuCl4{\cdot}3H_2O$), hydrochloric acid (HCl), nitric acid (HNO_3), thionyl chloride ($SOCl_2$), triethylamine (TEA), dichloromethane (DCM), hexane (HEX), tetrahydrofuran (THF), petroleum ether (PE), Tween 80 andethyl acetate (EA) were obtained

from Sinopharm Chemical reagent Co., Ltd (Shanghai, China). Biotin-poly (ethylene glycol)-lipoic acid (biotin-PEG-LA, MW = ~2000Da) and methoxyl poly (ethylene glycol)-lipoic acid (mPEG-LA, MW = ~2000Da) were purchased from Ponsure Biotechnology (Shanghai, China). Paclitaxel (PTX) was purchased from Ziyun Biotechnology Co., Ltd, (Yunnan, China). Lipoic acid (LA), 4-(dimethylamino) pyridine (DMAP), glutathione (GSH) and *N*-(3-dimethylaminopropyl)-*N*-ethyl-carbodiimide hydrochloride (EDC·HCl) were purchased from Aladdin reagent Co., Ltd (Shanghai, China). Acetonitrile (HPLC grade) was purchased from CINC High Purity Solvents (Shanghai) Co.,Ltd. Trifluoroacetic acid (TFA, HPLC grade) was bought from J&K Chemicals (Beijing). Other chemicals were analytically pure and used as received unless otherwise specified. Water was purified by distillation, deionization, and reverse osmosis (Milli-Q plus).

Breast cancer cell lines MCF-7 and MCF-7/ADR (multidrug resistant) were generously donated by Shanghai Institute of Material Medica, Chinese Academy of Sciences. Penicillin-streptomycin, RPMI-1640 medium, fetal bovine serum (FBS), 0.25% (w/v) trypsin-0.03% (w/v) ethylenediaminetetraacetic acid (EDTA) solution and phosphate buffer solution (PBS) were purchased from Gibco BRL (Gaithersburg, MD, USA).

2.2. Preparation of CTAB capped GNRs

CTAB capped GNRs (abbreviated as CTAB-GNRs) with a maximum optical absorption peak at 808 nm were synthesized by the seed-mediated approach [32]. Firstly, the seed solution was prepared by blending 5 mL of 0.2 M CTAB solution with 5 mL of 0.5 mM $HAuCl_4$ solution, followed by adding 0.6 mL fresh ice-cold aqueous solution of $NaBH_4$ (0.01 mM). Then the mixture was stirred vigorously for 2 min and kept undisturbed in a water bath at 30 °C for 2 h before use. For preparing the growth solution, 1.080 g CTAB and 0.0612 g 7-BrHNA were dissolved in 30 mL warm water and the solution was kept in a water bath at 30 °C after adding 0.96 mL $AgNO_3$ (4 mM). After being settled for 15 min, 30 mL $HAuCl_4$ (1 mM) and 0.1 mL HCl (37%) were added and stirred slowly for 15 min. Afterward, 0.3 mL L-ascorbic acid (0.1 M) was added and the mixture was stirred vigorously for 1 min. Finally, 96 μL of the seed solution was injected into the growth solution and was stirred for 30 s. For GNRs growth, the resultant mixture was kept constant in a water bath at 30 °C for 12 h. Gold nanorods were purified by centrifugation to remove remaining CTAB (three times at 10, 000 rpm, 10 min each). The precipitates were collected and then dispersed in water.

2.3. Synthesis of PTX-LA and CUR-LA

Synthesis of PTX-LA is schematically represented in Fig. 2A. A solution of lipoic acid (103.2 mg, 0.5 mmol)in 5 mL of DCM were added to EDC•HCl (95.9 mg, 0.5 mmol)and DMAP (61.1 mg, 0.5 mmol)followed by paclitaxel (427 mg, 0.5 mmol)pre-dissolved in 5 mL of DCM. After being stirred for 24 h at room temperature, the reaction mixture was poured into 30 mL of water. The organic phase was collected, washed with sodium bicarbonate and brine, and dried over sodium sulfate. After removing DCM by rotary evaporation, the obtained PTX-LA was purified by column chromatography on a silica gel with a mobile phase of EA-HEX (3:2, v/v).

Synthesis of CUR-LA is schematically shown in Fig. 2B. To synthesize CUR-LA, lipoic acid was activated. Lipoyl-chloride was prepared by adding dropwise1mL $SOCl_2$ to 5 mL DCM solution of lipoic acid (103 mg, 0.5 mmol) and stirred at room temperature for 1 h. DCM and excess $SOCl_2$ were removed by rotary evaporation and 5 mL THF was added to prepare the lipoyl-chloride solution. Afterward, the lipoyl-chloride solution was added dropwise to 10 mL THF solution of curcumin (185 mg, 0.5 mmol)under N_2 atmospheres in ice bath, followed by injection of 0.2 mL of TEA. After stirring overnight, the reaction solution was filtered and the filtrate was evaporated under reduced pressure. The obtained CUR-LA was purified by column chromatography on a silica gel with a mobile phase of PE-EA (3:2, v/v).

The chemical structure was confirmed by ^{1}H NMR recorded on a Varian Mercury Plus-400 NMR spectrometer (Varian, USA).

2.4. Fabrications of BPGNRs and PTX/CUR@BPGNRs

To prepare BPGNRs, mPEG-LA and biotin-PEG-LA (at the mass ratio of 4:1) was dissolved in 2 mL of water, followed by mixing with 1 mL of concentrated CTAB-GNRs. The mixture was stirred at room temperature for 24 h and centrifuged at 10, 000 rpm for 10 min three times to remove residual reactants. The obtained precipitate was re-dispersed in water before use. UV–Vis–NIR spectrophotometer and Zetasizer Nano ZS/ZEN3600 were also used to characterize BPGNRs.

A series of PTX/CUR@BPGNRs loading dual drugs in precisely controlled mass ratios were prepared by adding PTX-LA and CUR-LA in different mass ratios (PTX-LA: CUR-LA = 1:0.619, 1:0.929, 1:1.238, 1:2.477; corresponding PTX: CUR = 1:0.5, 1:0.75, 1:1, 1:2) to 40 μg/mL BPGNRs. The mixture was stirred at room temperature for 24 h. The resulting PTX/CUR@BPGNRs were centrifuged, washed and re-dispersed in water. PTX loaded BPGNRs (PTX@BPGNRs) and CUR loaded BPGNRs (CUR@BPGNRs) were prepared by a similar method. The mixture of PTX@BPGNRs and CUR@BPGNRs with the mass ratio of PTX and CUR at 1:1 was prepared by mixing PTX@BPGNRs containing 20 μg/mL PTX and CUR@BPGNRs containing 20 μg/mL CUR in equal volumes.

2.5. Characterization of CTAB-GNRs, BPGNRs and PTX/CUR@BPGNRs

UV–Vis–NIR spectrophotometer (Hitachi U-2910, Japan) and Zetasizer Nano ZS/ZEN 3600 (Malvern Instruments, Herrenberg, Germany) were used to characterize CTAB-GNRs, BPGNRs and PTX/CUR@BPGNRs. Their morphologies were observed on a transmission electron microscopy (TEM) (JEM-2100F, JEOL, Japan).

To obtain the drug loading capacities (DLCs) and encapsulation efficiencies (EEs) of PTX@BPGNRs, CUR@BPGNRs and PTX/CUR@BPGNRs, the supernatants during centrifugation were merged for the determination of free PTX-LA and CUR-LA content by HPLC. DLCs and EEs were calculated according to Eq. (1) -(4):

$$\mathrm{DLC_{PTX}}(\%) = \frac{MW_{PTX}}{MW_{PTX-LA}} \times DLC_{PTX-LA} = \frac{MW_{PTX}}{MW_{PTX-LA}} \times \frac{W_{PTX-LA} - w_{PTX-LA}}{M} \times 100 \quad (1)$$

$$\mathrm{DLC_{CUR}}(\%) = \frac{MW_{CUR}}{MW_{CUR-LA}} \times DLC_{CUR-LA} = \frac{MW_{CUR}}{MW_{CUR-LA}} \times \frac{W_{CUR-LA} - w_{CUR-LA}}{M} \times 100 \quad (2)$$

$$\mathrm{EE_{PTX}}(\%) = \frac{W_{PTX-LA} - w_{PTX-LA}}{W_{PTX-LA}} \times 100 \quad (3)$$

$$\mathrm{EE_{CUR}}(\%) = \frac{W_{CUR-LA} - w_{CUR-LA}}{W_{CUR-LA}} \times 100 \quad (4)$$

where *MW* is the molecular weight of each reagent, *W* is the total weight of the inputted reagent, *w* is the free drugs in the supernatants, and *M* is the total weight of the resulting drug loaded BPGNRs. The subscripts in the above equations are used to indicate which reagent the *MW*, *W and w* belong to.

2.6. Combinational effects of PTX and CUR

MTT (3-[4,5-dimethylthiazol-2-yl]-2,5-diphenyltetrazolium) assay was conducted to evaluate the cytotoxicity. Firstly, the MCF-7/ADR cells were tested for their drug resistance on PTX. In brief, MCF-7 and

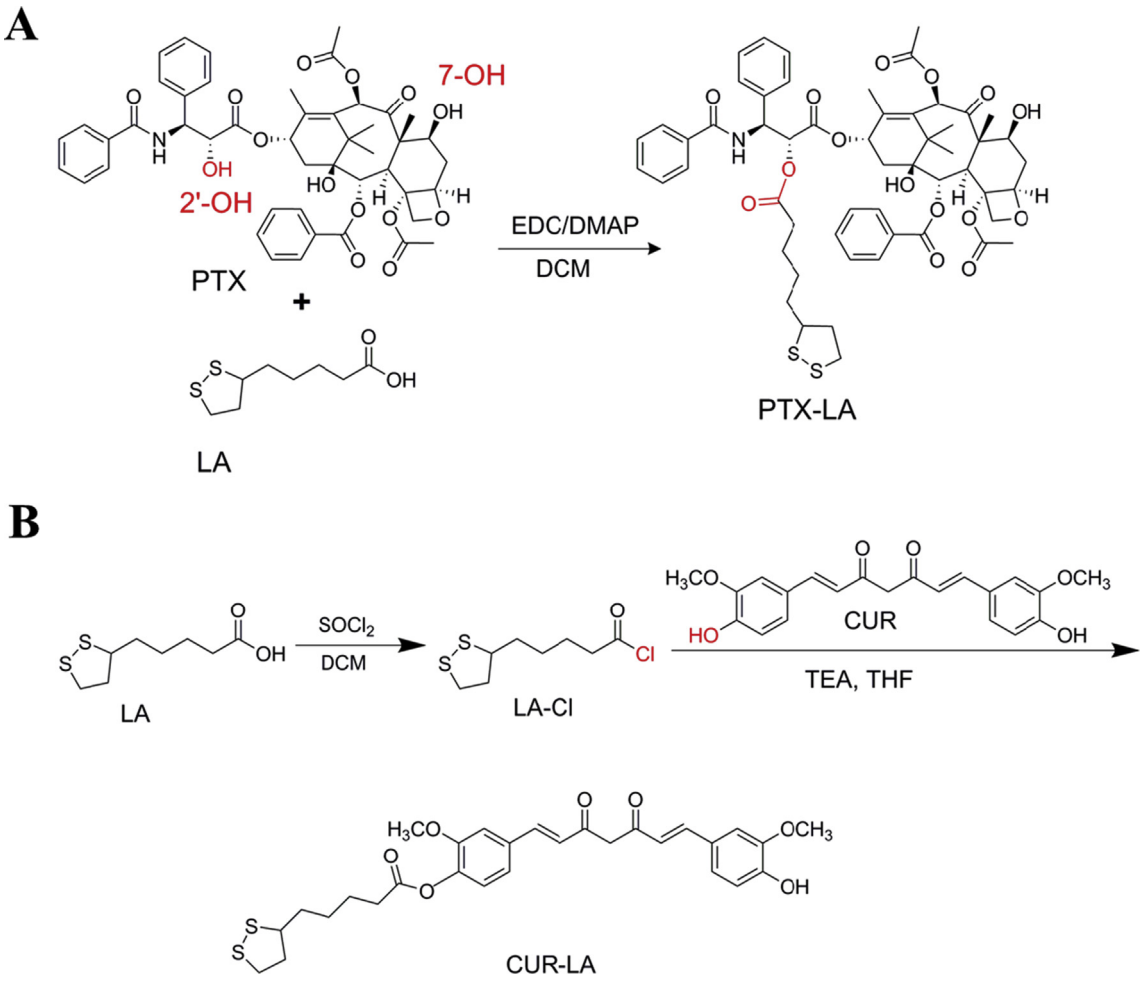

Fig. 2. Synthesis of PTX-LA(A) and CUR-LA (B).

MCF-7/ADR cells were seeded in 96-well plates at a density of 5000 cells/well and incubated for 24 h. Then the cells were treated with different concentrations of free PTX. After 48 h of incubation, the medium in each well was replaced with 200 μL of 0.5 mg/mL MTT. After 4 h of incubation, the medium containing MTT was removed and 200 μL of DMSO was added followed by oscillation in the dark for 10 min. The absorbance was determined at 570 nm by a microplate reader (Bio-Rad 680, USA). The 50% inhibitory concentrations (IC_{50}) of different samples were calculated by SPSS 21.0 software.

Next, we investigated the synergistic effects of free PTX and CUR combinations on MCF-7/ADR cells by MTT assay. The MCF-7/ADR cells were treated with different concentrations of free PTX, free CUR and combinations of free PTX and CUR with different mass ratios (PTX: CUR = 1:0.5, 1:0.75, 1:1, 1:2) for 48 h. The remaining steps were operated using the same procedure as previously described.

Afterward, we explored the synergistic effects of the PTX and CUR in PTX/CUR@BPGNRs on MCF-7/ADR cells. Similarly, MCF-7/ADR cells were seeded in 96-well plates at a density of 5000 cells/well and incubated for 24 h. Then the MCF-7/ADR cells were treated with different concentrations of PTX/CUR@BPGNR with different mass ratios between PTX and CUR (PTX: CUR = 1:0.5, 1:0.75, 1:1, 1:2; corresponding to PTX-LA: CUR-LA = 1:0.619, 1:0.929, 1:1.238, 1: 2.477) for 48 h. The remaining steps were operated using the same procedure as previously described.

To evaluate the combinational effects of PTX and CUR, the combination index (CI) was calculated based on the Chou and Talalay method [33]. The CI values were calculated according to Eq. (5):

$$CI = \frac{(D)1}{(D_{50})1} + \frac{(D)2}{(D_{50})2} \quad (5)$$

where $(D)_1$ and $(D)_2$ are the IC_{50} values of PTX and CUR in combination therapy, $(D_{50})_1$ and $(D_{50})_2$ are the IC_{50} values of free PTX and free CUR alone, respectively. Based on the method, CI < 1 suggests synergistic effects, CI = 1 suggests additive effects, and CI > 1 suggest antagonistic effects.

2.7. Cytotoxicity

To evaluate the cytotoxicities of BPGNRs and the combinations of free PTX and free CUR (free PTX/CUR) with or without NIR irradiation, MCF-7/ADR cells (5000 cells per well) were seeded in 96-well plates and incubated for 24 h. Then the cells were treated with BPGNRs and free PTX/CUR at various concentrations for 8 h. Then, the cells were treated with or without NIR irradiation (2.5 W/cm^2) for 10 min. After further incubation for 40 h, the cell viabilities were determined by the MTT assay.

Cytotoxicity of single drug loaded BPGNRs (PTX@BPGNRs and CUR@BPGNRs) and the physical mixtures PTX@BPGNRs and CUR@BPGNRs with a PTX/CUR ratio at 1:1 (the preparation was described above, see 2.4) were also investigated by MTT assay. The resistance reversal index (RRI) = IC_{50} value of free PTX/IC_{50} value of PTX in drug loaded BPGNRs.

2.8. Cellular uptake

Cellular uptake of the PTX/CUR@BPGNRs was measured with

inductively coupled plasma mass spectrometry (ICP-MS, iCAP Q, Germany). MCF-7/ADR cells (1×10^6 cells/well) were seeded in 6-well plates and incubated for 24 h. Then the medium was replaced with PTX/CUR@BPGNRs containing 2.5 μg/mL of PTX and CUR with 40 μg/mL BPGNRs and the cells were incubated for 2, 4, 8, 12 and 24 h. At the predetermined time, the cells were digested with trypsin and washed with ice-cold PBS to remove the extracellular PTX/CUR@BPGNRs. Subsequently, the cells were stained with 0.4% trypan blue and the living cells were counted under inverted microscope (Olympus BX51, Japan). The cells were digested by aqua regia ($HCl/HNO_3 = 3:1$, v/v) overnight and the aqua regia was volatilized to dryness in a draught cupboard. Finally, the residues were dissolved in 2% HNO_3 and determined by ICP-MS.

2.9. In vitro drug release

0.2 mL condensed PTX/CUR@BPGNRs was placed in dialysis bags (MWCO = 3500 Da). After sealed tightly with threads, the dialysis bags were immersed into 10 mL of the following release media: (1) PBS (pH 7.4) with Tween 80 (0.5%, w/v); (2) PBS (pH 7.4) with Tween 80 (0.5%, w/v) under NIR irradiation of power intensity at 2.5 W/cm^2 for 10 min at the predetermined time points; (3) PBS (pH 7.4) with Tween 80 (0.5%, w/v) containing 5 μM GSH; (4) PBS (pH 7.4) with Tween 80 (0.5%, w/v) containing 5 mM GSH; (5) PBS (pH 7.4) with Tween 80 (0.5%, w/v) containing 30 U/mL PLE; (6) PBS (pH 7.4) with Tween 80 (0.5%, w/v) containing 5 mM GSH and 30 U/mL PLE. Then the above release media was placed in a shaking water bath (37 °C, 100 rpm) for 72 h. At predetermined time intervals, 0.1 mL of the release medium was taken out for HPLC analysis and the equal volume of fresh medium was supplemented. The 10 min NIR irradiation was exerted soon after the fresh medium was added.

2.10. Intracellular drug release

MCF-7/ADR cells (5×10^5 cells/well) were seeded in 12-well plates and incubated for 12 h. Then the medium was replaced with fresh medium containing free PTX/CUR or PTX/CUR@BPGNR. The mass ratios between PTX and CUR in these two group were 1:1 and the final concentration was 2.5 μg/mL. Then the cells were incubated for 2, 4, 8 and 12 h. At the end of incubation, cells were digested by trypsin and washed with ice-cold PBS. Cells were freeze-thawed to lyse cells and release the drugs. The cell lysates were centrifuged at 10, 000 rpm for 10 min to collect the supernatant. The supernatant was separated into two parts, one was used to determine the total cell protein amount by the BCA Protein Assay Kit (Beyotime, China), and the other was subjected to HPLC analysis for the content of PTX and CUR. The intracellular contents of PTX and CUR were normalized to the total protein amount.

2.11. Cell apoptosis

The cell apoptosis was quantitative analyzed by Annexin V-FITC/PI Apoptosis Detection Kit (Beyotime, China). MCF-7/ADR cells (5×10^5 cells/well) were seeded in 12-well plates and incubated for 24 h. Then the cells were treated with free PTX/CUR, PTX/CUR@BPGNR, and PTX/CUR@BPGNR + NIR. The mass ratio between PTX and CUR in these groups were 1:1 and the final concentration was 2.5 μg/mL. Untreated cells were also tested for control. The NIR irradiation for 10 min was employed after 8 h incubation with PTX/CUR@BPGNR and the cells were further incubated for 40 h. The cells were collected after digestion and wash. 195 μL binding buffer, 5 μL Annexin-VFITC (fluorescein isothiocyanate) and 10 μL PI (Propidium Iodide) were added to each sample and mixed gently. Then the cell suspension was incubated in the dark for 15 min at room temperature followed by addition of 200 μL binding buffer. Finally, the samples were detected by the BD LSR Fortessa flow cytometry (Becton Dickinson, USA).

2.12. P-gp expression

P-gp expression of MCF-7/ADR cells was detected using a Human permeability glycoprotein (P-gp) ELISA Kit (Beijing BaiaoLaibo Technology, China). Firstly MCF-7/ADR cells (5×10^5 cells/well) were seeded in 12-well plates and incubated for 24 h. Then the medium was discarded and the cells were treated with free PTX, free PTX/CUR, PTX/CUR@BPGNR, and PTX/CUR@BPGNR + NIR. The mass ratio between PTX and CUR in these groups were 1:1 and the final concentration was 2.5 μg/mL. Untreated cells were also tested for control. The NIR irradiation for 10 min was employed after 8 h incubation with PTX/CUR@BPGNR. After further incubation for 40 h, the cells were digested and washed with ice-cold PBS. Then 1×10^6 cells in each group were collected and split by freezing and thawing. The cell lysate was centrifuged and the supernatant was extracted for the P-gp analysis following the manufacturer's protocol. The P-gp level was expressed as percent relative to the untreated group.

2.13. Statistical analysis

Data were expressed as the mean ± standard deviation (SD). Statistical analysis was performed using one-way ANOVA. The statistical difference between the data of two groups was considered to be significant when $p < 0.05$.

3. Results and discussion

3.1. Synthesis and characterization of PTX-LA and CUR-LA

In order to enable the conjugation of drugs to GNRs, lipoic acid (a kind of carboxylic acid containing sulfur atoms) was first used to esterify the drugs. The similar ester bonds allow PTX-LA and CUR-LA to be hydrolyzed to release free drugs simultaneously. As illustrated in Fig. 2, PTX-LA was synthesized via an EDC/DMAP coupling reaction. Then the reaction mixture was purified with column chromatographic separation under the monitoring of thin layer chromatography (TLC). The chemical identities of PTX-LA were confirmed by ^{1}H NMR spectrum. Compared with the ^{1}H NMR spectra of LA (Fig. 3A) and PTX (the upper one in Fig. 3B), characteristic peaks of PTX and LA were observed in the ^{1}H NMR spectrum of PTX-LA (the lower one in Fig. 3B), indicating the successful conjugation of LA and PTX. It is noteworthy that the resonance at $\delta = 4.8$ ppm (s, 1H), which is assigned to the proton of the 2′-OH, was observed in the spectrum of PTX (the red arrow in Fig. 3B) and not observed in the spectrum of PTX-LA. This difference suggested that LA was conjugated at this position. Besides, we also found that the 2′-OH was more active than 7-OH, perhaps due to the larger steric hindrance around the 7-OH.

For the synthesis of CUR-LA, LA was first reacted with $SOCl_2$ to generate lipoic chloride (LA-Cl). Afterward, CUR was coupled to LA to obtain CUR-LA where triethylamine (TEA) was used as a base. Finally, silica gel column chromatography was used to separate and purify CUR-LA from the reaction mixture with TLC analysis. The ^{1}H NMR spectrum of CUR and CUR-LA were shown in Fig. 3C and D, respectively. In ^{1}H NMR spectrum of CUR-LA, characteristic peaks of CUR (Ph-: $\delta = 7.17$–6.92, and CH3-: $\delta = 3.97$–3.83) and LA (-S-CH-CH2-: $\delta = 3.59$, the peak b in Fig. 3D; -S-CH2-CH2-: $\delta = 3.15$, the peak a in Fig. 3D) were both observed. Moreover, the molecular masses of CUR-LA and PTX-LA were determined to be 557.1661 $[M+H]^+$ and 1043.3760 $[M+H]^+$ respectively (Fig. S1), which are accorded with the predicted molecular formulas: $C_{29}H_{32}O_7S_2$ for CUR-LA and $C_{55}H_{63}NO_{15}S_2$ for PTX-LA. These data verified that CUR-LA and PTX-LA had been successfully synthesized.

3.2. Characterization of CTAB-GNRs, BPGNRs and PTX/CUR@BPGNRs

Firstly, the CTAB-capped GNRs were prepared using the seed

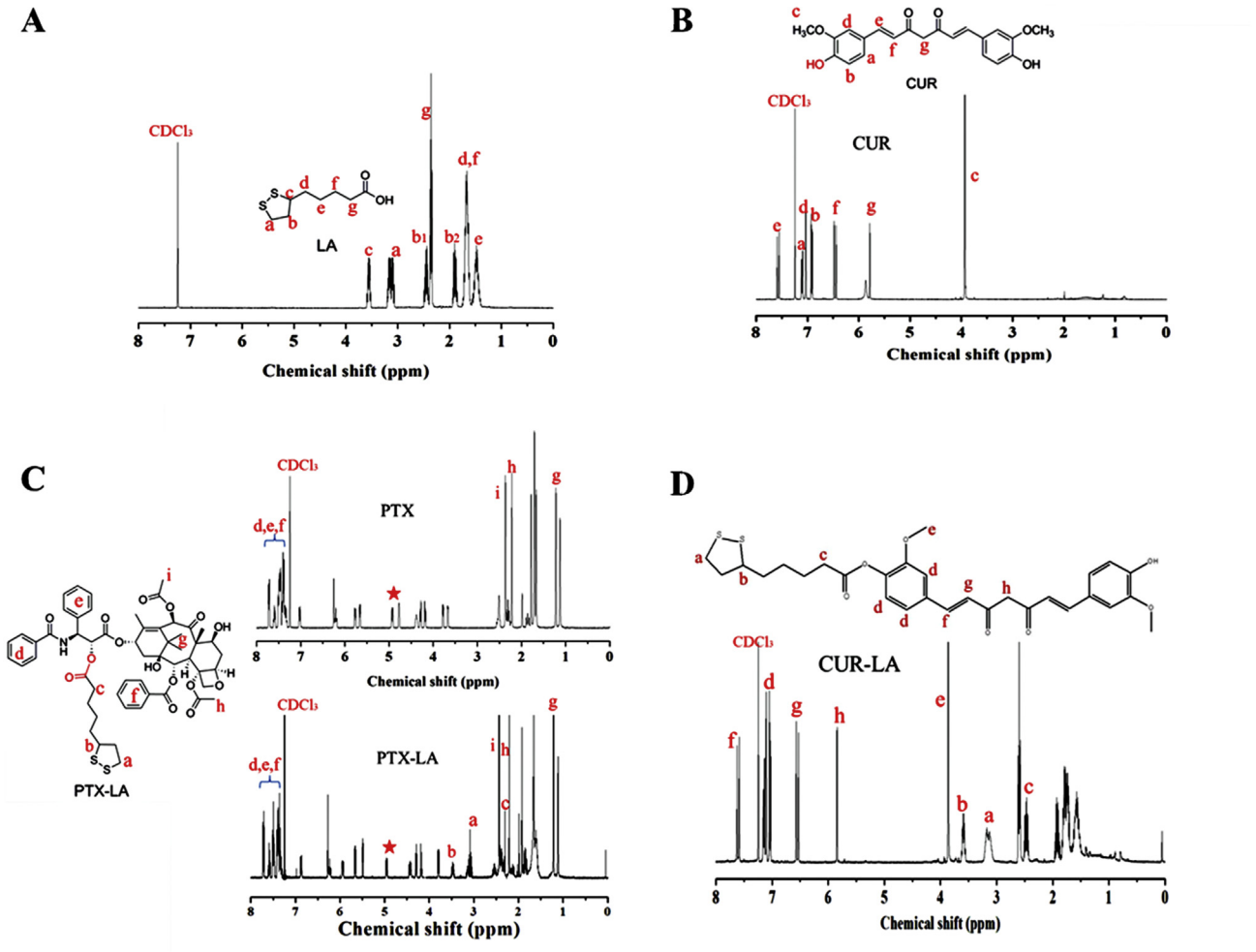

Fig. 3. ^{1}H NMR spectra of LA (A), PTX and PTX-LA (B), CUR (C), CUR-LA (D).

growth method. Then they were treated with PEG-LA and Biotin-PEG-LA to replace surface CTAB surfactants to obtain biotin-PEG modified GNRs (BPGNRs). Finally, PTX-LA and CUR-LA were loaded onto the BPGNRs to prepare PTX/CUR@BPGNRs via Au–S bond.

Fig. 4A compares UV–Vis–NIR absorption spectra of CTAB-GNRs, BPGNRs and PTX/CUR@BPGNRs. The typical characteristics of CTAB-GNRs solution were shown in the spectra: two surface plasma resonances (SPR) absorption peaks corresponding to the longitudinal (LSPR) at 808 nm and transverse (TSPR) at 510 nm. Compared with original GNR stabilized with CTAB, there were negligible changes in the absorption spectra of BPGNRs and PTX/CUR@BPGNRs, indicating the unique optical properties of GNRs were well-maintained after the surface modifications. And the resulting PTX/CUR@BPGNRs showed an LSPR peak at 809 nm, suggesting its excellent absorption property under NIR irradiation of 808 nm. Zeta potential measurements resulted in values of -5.53 ± 0.73 mV for BPGNRs and -3.97 ± 0.52 mV for PTX/CUR@BPGNRs in contrast with $+40.37 \pm 2.48$ mV for CTAB capped GNRs (Fig. 4B), as a confirmation of successful modification of the GNR surface.

As shown in Fig. 4C and D, the CTAB-GNRs and PTX/CUR@BPGNRs have similar rod-shape and size. The PTX/CUR@BPGNRs had an aspect ratio of ~3.9, which averaged 50.2 nm in length and 12.9 nm in width. The PTX/CUR@BPGNRs were dispersed in water, PBS (pH 7.4) and cell culture medium. After 5 days standing, the mediums were still transparent without any agglomeration or precipitation (Fig. S2), indicating a good colloidal stability of PTX/CUR@BPGNRs in the above three mediums.

3.3. Precisely ratiometric control over dual-drug loading

For controlled loading different drugs in the same nanoparticle, high and homogeneous encapsulation efficiency for every drug is imperative. PTX and CUR were loaded onto BPGNRs via the same robust Au–S bonds with high binding efficiency. In our preliminary experiments, we prepared different concentrations of single drug loaded and dual drug loaded BPGNRs, finding a constant encapsulation efficiency (approximately 85%) of PTX-LA and CUR-LA when drug concentrations were no more than 40 μg/mL and BPGNR concentration was fixed at 40 μg/mL.

Based on the results, we loaded PTX-LA and CUR-LA with the mass ratio of 1:1.238 (the corresponding mass ratio of PTX and CUR is 1:1) onto BPGNRs to obtain the PTX/CUR@BPGNRs (1:1). As shown in Table 1, the EEs of PTX-LA and CUR-LA in PTX/CUR@BPGNRs (1:1) were 85.3% and 85.0%, while the DLCs were 6.49% and 7.83%, respectively. The DLCs of PTX and CUR were calculated by converting the DLSs of PTX-LA and CUR-LA with the molecular weight proportions. The DLCs of PTX and CUR were 5.32% and 5.21%, respectively. Therefore, the loading ratio between PTX and CUR was 1: (0.976 ± 0.05) (w/w) which is almost identical with the initial feeding ratio of PTX and CUR (1:1). These results affirmed that PTX and CUR were precisely ratiometric co-loaded to the same BPGNRs.

3.4. Combinational effects of PTX and CUR

The IC_{50} values of PTX against MCF-7 cells and MCF-7/ADR cells were calculated to investigate the levels of MDR. The results showed

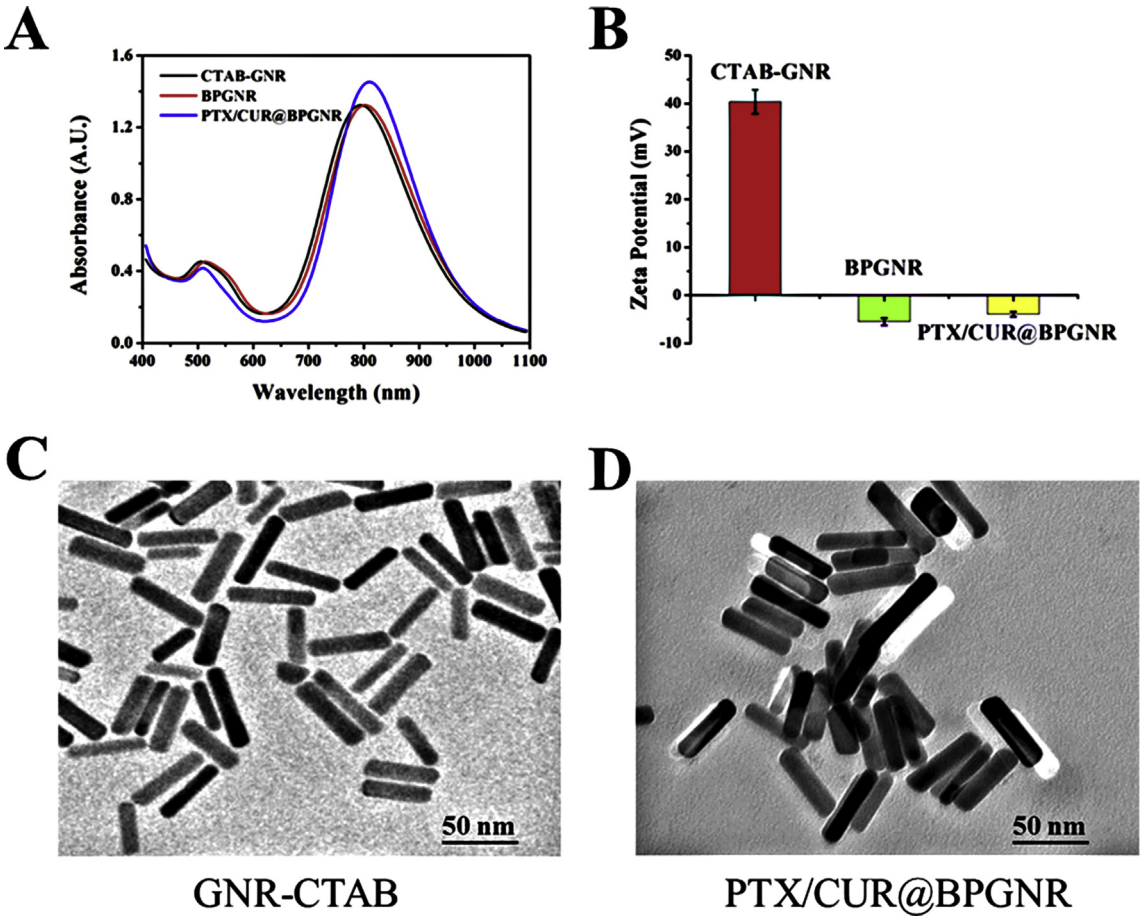

Fig. 4. Characterizations of GNR-based systems. UV–Vis–NIR absorption spectra (A) and Zeta potential (B) of CTAB-GNRs, BPGNRs and PTX/CUR@BPGNRs. TEM images of CTAB-GNRs (C) and PTX/CUR@BPGNRs (D).

Table 1
Drug loading capacities (DLCs) and encapsulation efficiencies (EE) of PTX-LA, CUR-LA, PTX and CUR for the PTX/CUR@BPGNRs (1:1).

Drug	DLCs (%)	EEs (%)
PTX-LA	6.49 ± 0.21	85.3% ± 1.53
CUR-LA	7.84 ± 0.16	85.0% ± 1.86
PTX	5.32 ± 0.27	
CUR	5.21 ± 0.32	

Table 2
IC_{50} and CI Values of different treatments in MCF-7/ADR cells after 48 h incubation.

Treatment	IC_{50} (μg/mL)		CI
	PTX	CUR	
Free PTX	20.17	–	–
Free CUR	–	34.16	–
Free PTX: CUR (1:0.5)	12.24	6.12	0.786
Free PTX: CUR (1:0.75)	9.80	7.35	0.701
Free PTX: CUR (1:1)	9.73	9.73	0.767
Free PTX: CUR (1:2)	7.31	14.62	0.790
PTX/CUR@BPGNRs (1:0.5)	2.74	1.37	0.176
PTX/CUR@BPGNRs (1:0.75)	2.36	1.77	0.169
PTX/CUR@BPGNRs (1:1)	1.84	1.84	0.145
PTX/CUR@BPGNRs (1:2)	1.41	2.82	0.152

The ratio in the bracket presents the mass ratio between PTX and CUR.

that IC_{50} value of MCF-7/ADR cells was relatively high (20.17 μg/mL), which was 150-fold higher than the parent MCF-7 cells (IC_{50} = 0.134 μg/mL). Therefore, the MCF-7/ADR cells were highly drug-resistant to PTX and could be used for the following experiments.

The combinational effects of drug combinations based on free form of PTX and CUR with different mass ratios were investigated. IC_{50} values of free PTX, free CUR and combinations of free PTX and CUR (free PTX/CUR) with the mass ratio of 1:0.5, 1:0.75, 1:1 and 1:2 against MCF-7/ADR cells and the CIs were displayed in Table 2. The CI values of all the tested combinations of free drugs were all less than 1, suggesting the combination of PTX and CUR could bring out notable synergistic effects. More importantly, the results showed that free PTX/CUR with a mass ratio of 1:0.75 exhibited the strongest synergism among the four series of combinations of free PTX and CUR.

The CI values of PTX/CUR@BPGNRs with different mass ratios between PTX and CUR were also shown in Table 2. Interestingly, for PTX/CUR@BPGNRs, we found that the mass ratio of 1:1 resulted in the strongest synergistic effects among four tested mass ratios, which was different from that of free PTX/CUR. The main reason for the discrepancy could be that the ways of drugs entered into MCF-7/ADR cells are different. The free drugs enter cells through diffusion, which is related to physicochemical properties of drugs. Free PTX and CUR may lead to different uptake behaviors, as a result, mass ratio of drugs inside cells may be inconsistent with the initial mass ratio. As for the PTX/CUR@BPGNRs, which has been modified with biotin, can bind with the overexpressing biotin receptor on tumor cell membrane [19–21]. The binding could result in receptor mediated endocytosis which internalize the PTX/CUR@BPGNR as a whole and maintain the loading mass ratio.

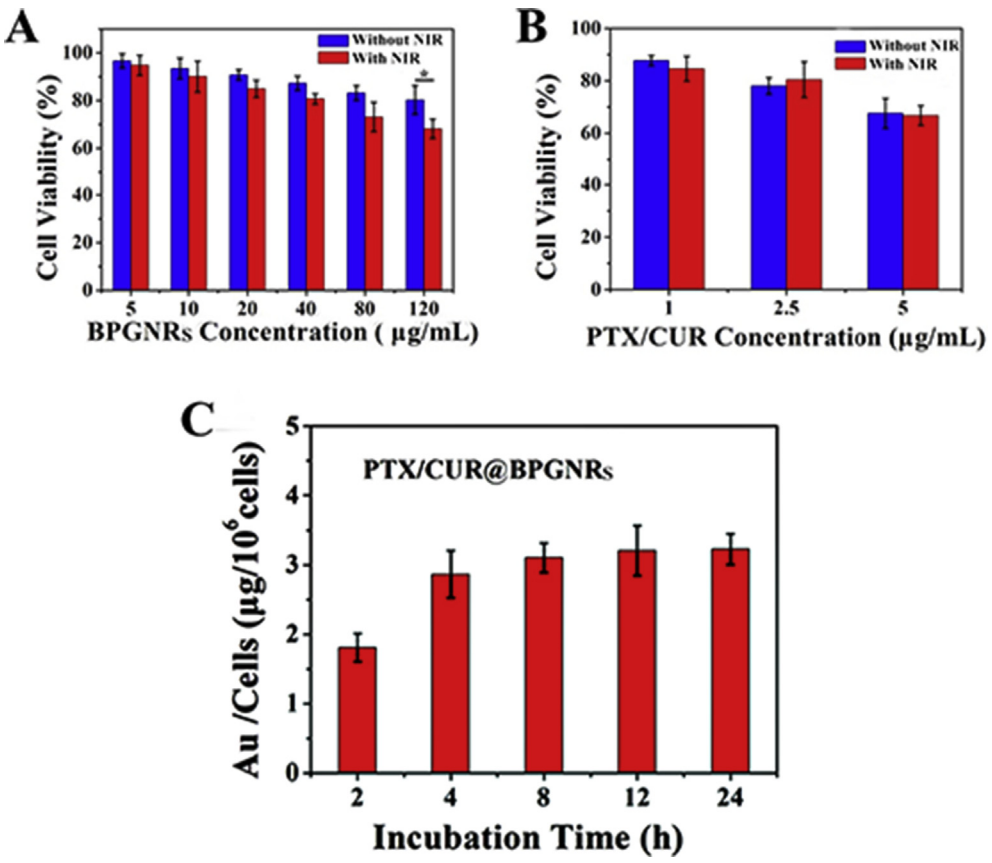

Fig. 5. A: Cell viabilities of MCF-7/ADR cells incubated with different concentrations of BPGNRs with and without NIR irradiation (*: $p < 0.05$). B: Cell viabilities of MCF-7/ADR cells incubated with combinations of free PTX and CUR (1:1) at different concentrations with and without NIR irradiation. C: Quantification of gold nanorods per million cells determined by ICP-MS after incubation for 2 h, 4 h, 8 h 12 h and 24 h. The NIR irradiation was performed with the laser power intensity at 2.5 W/cm^2 for 10 min. (For interpretation of the references to colour in this figure legend, the reader is referred to the Web version of this article.)

3.5. Cytotoxicity

In the view of the best synergist effect, we selected the PTX/CUR@BPGNRs (1:1) which load PTX and CUR with a mass ratio of 1:1 for the following research. To clarify its cytotoxicity, we evaluated the cytotoxicities of BPGNRs, free PTX and free CUR with or without NIR irradiation firstly. As can be seen from Fig. 5A, negligible cytotoxicity was observed in a certain concentration range (1–120 μg/mL), with over 80% cell viability when BPGNRs concentration reached 120 μg/mL after 48 h of incubation, indicating that BPGNRs possessed good biocompatibility for MCF-7/ADR cells. Fig. 5A also showed that NIR irradiation had an ignorable impact on cell viability when BPGNRs concentration was below 40 μg/mL, while the temperature reached about 42 °C (shown in Fig. S3), implying that the photothermal heating alone generated by the NIR radiation with 40 μg/mL of BPGNRs did not exceed cell killing threshold. However, cell viabilities decreased to below 75% where BPGNR concentration was 120 μg/mL under NIR irradiation, suggesting that the cytotoxicity of BPGNRs under NIR irradiation became obvious in high concentrations with the increasing temperature. Moreover, no obvious difference was found in the cell viabilities of MCF-7/ADR cells after incubation with free PTX and CUR with or without NIR irradiation (Fig. 5B). Finally, we continued the experiments with a BPGNRs concentration of 40 μg/mL.

Then the cytotoxicities of PTX@BPGNRs, CUR@BPGNRs, PTX@BPGNRs + CUR@BPGNRs (the mass ratio between the corresponding PTX and CUR was 1:1) and PTX/CUR@BPGNRs (1:1) against MCF-7/ADR cells were investigated. As shown in Table 3, the IC50 values of PTX and CUR in PTX@BPGNRs and CUR@BPGNRs against MCF-7/ADR cells were 5.65 and 12.98 μg/mL, respectively, both of which were much lower than that of their free forms, demonstrating enhanced cytotoxicities of the drugs loaded in BPGNRs as nanoformulations. Since we have proved that BPGNRs were not cytotoxic towards MCF-7/ADR cells (See Fig. 5A), the cytotoxicity of PTX/CUR@BPGNRs (1:1) could be attributed to the released drugs from the conjugates. In particular, the IC_{50} value of PTX/CUR@BPGNRs (1:1) was 1.84 μg/mL and the RRI of PTX/CUR@BPGNRs (1:1) was 10.96, indicating its strongest lethal effect on MCF-7/ADR cells.

Table 3
IC_{50} values and resistance reversal indexes (RRI) of different treatments against MCF-7/ADR cells.

Treatment	IC_{50} (μg/mL)	RRI
Free PTX	20.17	–
PTX@BPGNR	5.65	3.6
CUR@BPGNR	12.98	–
PTX@BPGNR + CUR@BPGNR (1:1)	1.96	10.29
PTX/CUR@BPGNR (1:1)	1.84	10.96

3.6. Cellular uptake

According to the reports, the cellular uptake characteristics of nanomaterials could be affected by their physicochemical properties and is significant for their biological applications [34–36]. Herein, ICP-MS was used to investigate the cellular uptake of PTX/CUR@BPGNRs. As shown in Fig. 5C, the gold content per million cells reached a plateau after 8 h of incubation, indicating that the endocytosis of PTX/CUR@BPGNRs (1:1) by MCF-7/ADR cells nearly reached equilibrium. Based on the results, we imposed NIR irradiation on MCF-7/ADR cells after 8 h of incubation with PTX/CUR@BPGNRs.

3.7. In vitro drug release

It was widely reported that the extracellular and intracellular microenvironment was quite different, which could be taken advantage for nanocarriers to selectively release inside cells to reduce premature

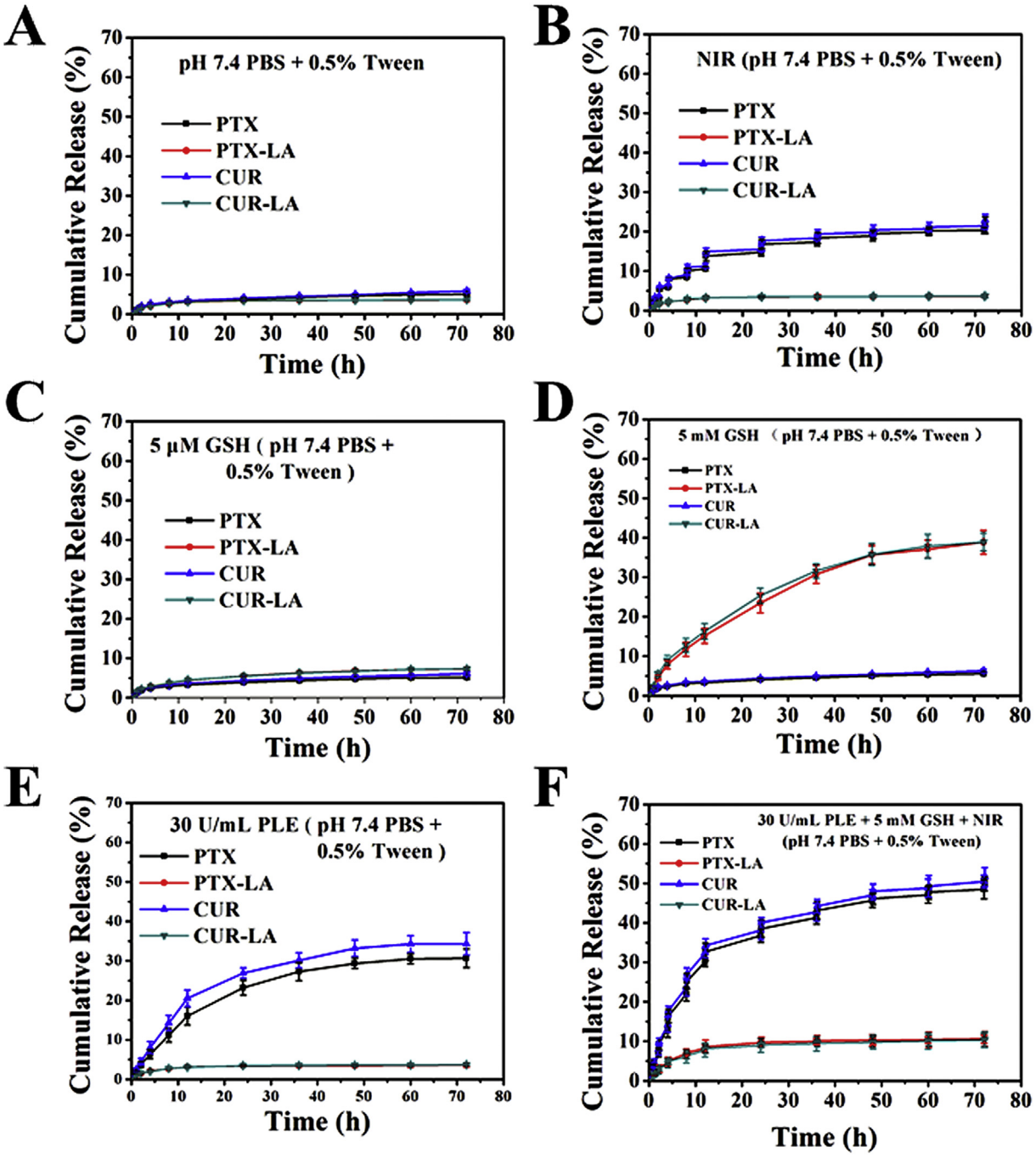

Fig. 6. Drug release profiles of PTX/CUR and PTX-LA/CUR-LA from the PTX/CUR@BPGNRs in following release media: PBS (pH 7.4) with Tween 80 (0.5%, w/v) (A); PBS(pH 7.4)with Tween 80 (0.5%, w/v) with NIR irradiation (B); PBS (pH 7.4) with Tween 80 (0.5%, w/v) containing 5 μM GSH (C); PBS (pH 7.4) with Tween 80 (0.5%, w/v) containing 5 mM GSH (D); PBS (pH 7.4) with Tween 80 (0.5%, w/v) containing 30 U/mL PLE (E); PBS (pH 7.4) with Tween 80 (0.5%, w/v) containing 5 mM GSH and 30 U/mL PLE with NIR irradiation (F). In all groups, the concentrations of free drugs and the drugs in PTX/CUR@BPGNRs were 2.5 μg/mL and the NIR was performed at laser power of 2.5 W/cm^2 for 10 min **: $p < 0.01$, ***: $p < 0.001$ compared with the corresponding amount of PTX, CUR, PTX-LA and CUR-LA released in PBS (pH 7.4) respectively.

drug leakage [24–27,37]. To reach this goal, besides the utilization of the biotin moiety as a targeting ligand, PTX/CUR@BPGNRs (1:1) were also designed with responses to the following stimuli: GSH, esterase and NIR photothermal effects. PTX-LA and CUR-LA were conjugated to BPGNRs via Au–S bonds [18]. Au–S bonds are relatively stable under low GSH concentration of extracellular environment but can be detached from the surface of GNRs under high GSH concentration in the cytoplasm of tumor cells [22–25]. The abundant intracellular esterase also enabled the specific release of PTX and CUR from PTX-LA and CUR-LA inside MCF-7/ADR cells [28,29]. Additionally, when PTX/CUR@BPGNRs were internalized by tumor cells, external NIR irradiation also contributed to the release of PTX and CUR by promoting the hydrolysis of ester bonds. The detached PTX-LA, CUR-LA and released PTX and CUR in different release media were measured by HPLC to characterize the in vitro release profiles.

The PTX/CUR@BPGNRs were first incubated in PBS at pH 7.4 containing 0.5% Tween. As shown in Fig. 6A, both free drugs (free PTX and CUR) and prodrugs (PTX-LA and CUR-LA) exhibited slow release

profiles in PBS at pH 7.4 (the cumulative release percentages of PTX, CUR, PTX-LA and CUR-LA were 3.88 ± 0.35%, 4.13 ± 0.48%, 3.62 ± 0.39% and 3.65 ± 0.25% at 72 h), indicating that PTX/CUR@BPGNRs were relatively stable at physiological conditions. Nevertheless, the release rates of free PTX and CUR were significantly increased once the NIR irradiation (2.5 W/cm^2 for 10 min) was given at predetermined time points (Fig. 6B). In detail, approximately 20% of free PTX and CUR were detected in the release media after 72 h of incubation. This could be due to the local heating generated by BPGNRs under NIR irradiation, which facilitated hydrolysis of the ester bonds of the prodrugs (PTX-LA, CUR-LA) conjugated to BPGNRs.

Next, we investigated the drug release profiles in PBS solutions containing different GSH concentrations (5 μM and 5 mM) to mimic extracellular and intracellular reduction environments, respectively. As shown in Fig. 6C and D, there was no obvious difference in the release profiles of free drugs (PTX and CUR) between the groups containing 5 μM and 5 mM GSH concentrations (the cumulative release percentages were no more than 6.5%). The amounts of released prodrugs were found to increase little (PTX-LA: 6.87 ± 0.35%, CUR-LA: 7.12 ± 0.25%) in the release media containing 5 μM GSH at 72 h, suggesting good stability of PTX/CUR@BPGNRs in extracellular reduction environment (Fig. 6C). By contrast, the amounts of detected prodrugs reached up to 38.54 ± 3.05% (for PTX-LA) and 38.93 ± 2.27% (for CUR-LA) after 72 h of incubation with a high concentration of GSH (Fig. 6D). It is reported that GSH can act as a reducing agent to exchange the therapeutic prodrugs from the surface of the gold. These data showed that the drugs were liberated from PTX/CUR@BPGNRs in the form of prodrugs by the GSH concentration-dependent thiol group exchange reaction.

It is generally accepted that esterase concentration inside tumor cells is 2–3 orders of magnitude higher than that in extracellular fluid[26]. Therefore, PLE was used to study the drug release in the simulated intracellular environment of tumor cells. As depicted in Fig. 6E, the amounts of released free PTX and CUR at 72 h were 30.67 ± 2.35% and 34.32 ± 2.89%, respectively. However, the cumulative percentage of released prodrugs (PTX-LA and CUR-LA) did not exceed 4% at 72 h. The results indicated that PTX/CUR@BPGNRs could be enzymatically hydrolyzed to release the free drugs through quick degradation of the ester linkage in the presence of a high concentration of esterase.

Most importantly, when PTX/CUR@BPGNRs were incubated with the release media 5 mM GSH and 30 U/mL PLE (simulated the intracellular environment of tumor cells) under intermittent NIR irradiation, we found that 49.89 ± 1.78% of PTX and 51.65 ± 2.37% of CUR were released from PTX/CUR@BPGNRs at 72 h (Fig. 6F). The hydrolysis of ester bonds in PTX-LA and CUR-LA caused by NIR and esterase result in the decrease of PTX-LA (10.61 ± 1.89%) and CUR-LA (10.42 ± 1.98%) in this media compared with that in media with 5 mM GSH alone. It is important that the released amount of PTX and CUR were almost same which in accordance with their loading ratio (1:1), suggesting the achievement of precise ratiometric co-release.

3.8. Intracellular drug release

MCF-7/ADR cells were incubated with combination of free PTX/CUR (1:1) and PTX/CUR@BPGNRs (1:1) for 2, 4, 8 and 12 h with corresponding PTX and CUR concentration of 2.5 μg/mL to study the intracellular release behavior of PTX and CUR from PTX/CUR@BPGNRs. As shown in Fig. 7A, the internalized amounts of PTX and CUR in the free PTX/CUR group and PTX/CUR@BPGNRs group both increased gradually during incubation. In free PTX/CUR group, the intracellular amount of PTX was less and increased much slower than that of CUR, indicating that PTX and CUR did not enter MCF-7/ADR cells simultaneously. This significant difference could be due to the more hydrophobic property of free CUR compared with free PTX, which was more conducive to the diffusion into cells. However, the mass ratio of intracellular released PTX and CUR was approximate 1:1 in PTX/CUR@BPGNRs group (no difference between the PTX amount and the CUR amount) at different time points, which was practically identical to the loading ratio between PTX and CUR in PTX/CUR@BPGNRs. It suggested that PTX/CUR@BPGNRs (1:1) co-delivered and co-released PTX and CUR at a predetermined ratio in MCF-7/ADR cells. We also observed that greater amount of PTX and CUR was delivered into MCF-7/ADR cells in PTX/CUR@BPGNRs group compared with those in free PTX/CUR group, showing a remarkable advantage of PTX/CUR@BPGNRs in efficient delivery of PTX and CUR.

3.9. Cell apoptosis

To quantify the apoptotic effects induced by PTX/CUR@BPGNRs, MCF-7/ADR cells were stained with Annexin V-FITC/PI Apoptosis Assay kit and analyzed by flow cytometry. The total apoptosis rate is the sum of late apoptosis percentage (Q2, upper right) and early apoptosis percentage (Q3, lower right). As shown in Fig. 7B and C, free PTX/CUR (1:1) induced 25.3 ± 1.3% cell apoptosis. And PTX/CUR@BPGNRs (1:1) induced higher apoptosis rate (50.8 ± 3.2%) than that of free PTX/CUR (1:1), which is in accordance with the results of the above presented MTT assay. For the PTX/CUR@BPGNRs group with an additional NIR irradiation, the percentage of apoptotic cells increased to 67.2 ± 4.3%, while the percentage of necrotic cells was about 0.1%, suggesting the promotion of cell apoptosis induced by the accelerated release of drugs rather than direct killing of the cells by photothemal effect.

3.10. P-gp expression

One of the primary causes of MDR in MCF-7/ADR cells is the elevated expression of P-gp, a drug efflux pump which pumps anti-tumor drugs out of cells, leading to the reduction of intracellular drug concentration below effective dose. CUR was reported to down-regulate P-gp expression, thus could decrease the efflux of intracellular anti-tumor drugs [38]. P-gp ELISA Kit was used to determine P-gp expression after different treatments and the P-gp expression of untreated MCF-7/ADR cells was used as control. As we can see from Fig. 7D, free PTX exhibited the highest P-gp expression (116.4 ± 7.8%), indicating that free PTX could up-regulate P-gp expression in MCF-7/ADR cells [39]. Compared with free PTX/CUR (84.2 ± 5.4%), the P-gp expression levels of PTX/CUR@BPGNRs (60.4 ± 10.3%) further declined. It was found that the P-gp expression of MCF-7/ADR cells treated with PTX/CUR@BPGNRs with NIR irradiation was the lowest (48.2 ± 7.5%) among all the groups, due to the promoted intracellular delivery and release of CUR.

4. Conclusion

In this work, we presented a novel approach to precisely ratiometric co-loading PTX and CUR at the optimum ratio by conjugating them onto the same GNRs to combat MDR. By esterifying PTX and CUR with LA, PTX-LA and CUR-LA were conjugated to the same gold nanorod with approximately 85% encapsulation efficiency, PTX/CUR@BPGNRs were successfully prepared. The drug loading capacities of PTX and CUR in PTX/CUR@BPGNRs were 5.32 wt % and 5.21 wt %, which were in accordance with the predetermined mass ratio of PTX and CUR at approximately 1:1. In vitro and intracellular drug release profiles revealed that PTX and CUR were controllably and synchronously released inside the tumor cells. The PTX/CUR@BPGNRs with the mass ratio of PTX and CUR at 1:1 exhibited superior cytotoxicity and greater synergy on MCF-7/ADR cells than the free PTX and CUR mixture. In addition, PTX/CUR@BPGNRs had enhanced inhibition of P-gp expression on MCF-7/ADR cells especially with NIR irradiation than the free PTX and CUR mixture. Overall, our study offers a solution to the problem of loading different drugs into the same drug-delivery platform with a precisely controlled ratio because this drug-carrier conjugation approach can be generalized to various drugs containing hydroxyl groups.

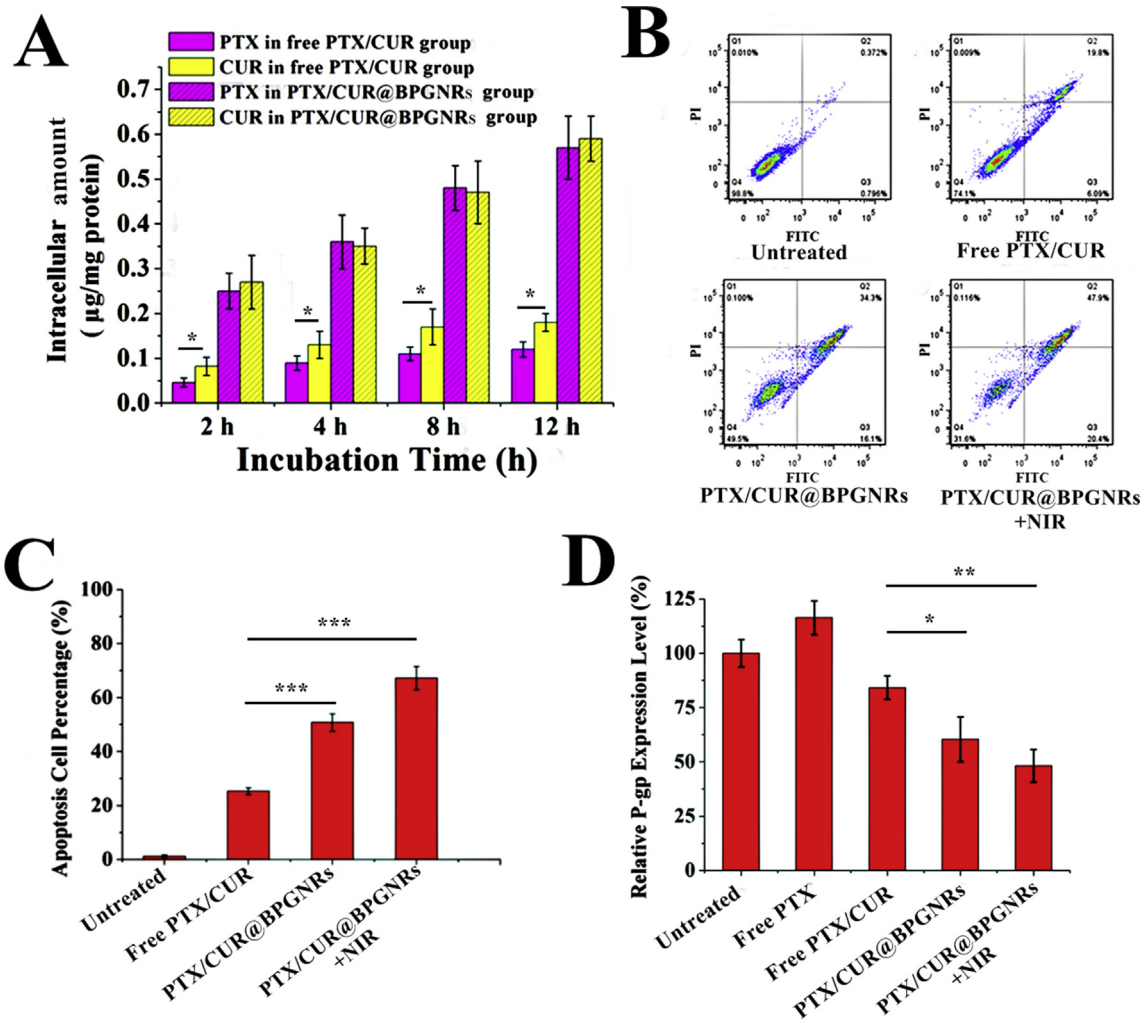

Fig. 7. Intracellular amounts of PTX and CUR (A), cell apoptosis analysis (B), cell apoptosis percentage (C), and relative P-gp expression level (D) of the MCF-7/ADR after treatments with none drug (untreated), free PTX, free PTX/CUR, PTX/CUR@BPGNRs and PTX/CUR@BPGNRs with NIR irradiation. In all groups, the drug concentrations of free drugs and the drugs in PTX/CUR@BPGNRs were both 2.5 μg/mL and the NIR was performed at laser power of 2.5 W/cm^2 for 10 min *: $p < 0.05$, **: $p < 0.01$, ***: $p < 0.001$.

Declaration of competing interest

The authors declare no competing financial interest.

Acknowledgements

We acknowledge financial supports from National Natural Science Foundation of China (grant numbers 81773647, 81771949), Medicine-Engineering Joint Foundation of Shanghai Jiao Tong University (grant numbers YG2014ZD01, YG2016MS28, YG2016MS17), Science and Technology Development Fund of Shanghai Pudong New Area (grant number PKJ2017-Y04), Shanghai Municipal Science and Technology Commission (grant number 17441901700) and Translational Medicine Foundation of Shanghai Jiao Tong University (grant number ZH2018ZDA03).

Appendix A. Supplementary data

Supplementary data to this article can be found online at https://doi.org/10.1016/j.jddst.2019.101383.

References

[1] C. Holohan, S. Van Schaeybroeck, D.B. Longley, P.G. Johnston, Cancer drug resistance: an evolving paradigm, Nat. Rev. Cancer 13 (2013) 714–726.
[2] N.C. Turner, J.S. Reis-Filh, Genetic heterogeneity and cancer drug resistance, Lancet Oncol. 13 (2012) e178–e185.
[3] Q. Hu, W. Sun, C. Wang, Z. Gu, Recent advances of cocktail chemotherapy by combination drug delivery systems, Adv. Drug Deliv. Rev. 98 (2016) 19–34.
[4] L. Miao, S. Guo, J. Zhang, W.Y. Kim, L. Huang, Nanoparticles with precise ratiometric co-loading and co-delivery of gemcitabine monophosphate and cisplatin for treatment of bladder cancer, Adv. Funct. Mater. 24 (2014) 6601–6611.
[5] P.G. Tardi, N. Dos Santos, T.O. Harasym, S.A. Johnstone, N. Zisman, A.W. Tsang, D.G. Bermudes, L.D. Mayer, Drug ratio-dependent antitumor activity of irinotecan and cisplatin combinations in vitro and in vivo, Mol. Cancer Ther. 8 (2009) 2266–2275.
[6] S. Aryal, C.M. Hu, L. Zhang, Combinatorial drug conjugation enables nanoparticle dual-drug delivery, Small 6 (2010) 1442–1448.
[7] L. Zhang, A.F. Radovic-Moreno, F. Alexis, F.X. Gu, P.A. Basto, V. Bagalkot, et al., Co-delivery of hydrophobic and hydrophilic drugs from nanoparticle-aptamer bioconjugates, ChemMedChem 2 (2007) 1268–1271.
[8] S. Aryal, C.M. Hu, L. Zhang, Polymeric nanoparticles with precise ratiometric control over drug loading for combination therapy, Mol. Pharm. 8 (2011) 1401–1407.
[9] S. Luo, Y. Gu, Y. Zhang, P. Guo, J.F. Mukerabigwi, M. Liu, S. Lei, Y. Cao, H. He, X. Huang, Precise ratiometric control of dual drugs through a single macromolecule for combination therapy, Mol. Pharm. 12 (2015) 2318–2327.
[10] E.C. Dreaden, A.M. Alkilany, X.H. Huang, C.J. Murphy, M.A. El-Sayed, The golden age: gold nanoparticles for biomedicine, Chem. Soc. Rev. 41 (2012) 2740–7279.
[11] A.M. Alkilany, L.B. Thompson, S.P. Boulos, P.N. Sisco, C.J. Murphy, Gold nanorods: their potential for photothermal therapeutics and drug delivery, tempered by the complexity of their biological interactions, Adv. Drug Deliv. Rev. 64 (2012) 190–199.
[12] L. Vigderman, B.P. Khanal, E.R. Zubarev, Functional gold nanorods: synthesis, self-assembly, and sensing applications, Adv. Mater. 24 (2012) 4811–4841.

[13] N. Wang, T. He, Y. Shen, L. Song, L. Li, X. Yang, X. Li, M. Pang, W. Su, X. Liu, Q. Wu, C. Gong, Paclitaxel and tacrolimus coencapsulated polymeric micelles that enhance the therapeutic effect of drug-resistant ovarian cancer, ACS Appl. Mater. Interfaces 8 (2016) 4368–4377.
[14] B.B. Aggarwal, S. Shishodia, Y. Takada, S. Banerjee, R.A. Newman, C.E. Bueso-Ramos, J.E. Price, Curcumin suppresses the paclitaxel-induced nuclear factor-kappaB pathway in breast cancer cells and inhibits lung metastasis of human breast cancer in nude mice, Clin. Cancer Res. 11 (2005) 7490–7498.
[15] O.S. Muddineti, P. Kumari, B. Ghosh, V.P. Torchilin, S. Biswas, d-α-Tocopheryl succinate/phosphatidyl ethanolamine conjugated amphiphilic polymer-based nanomicellar system for the efficient delivery of curcumin and to overcome multiple drug resistance in cancer, ACS Appl. Mater. Interfaces 9 (2017) 16778–16792.
[16] H.B. Ruttala, Y.T. Ko, Liposomal co-delivery of curcumin and albumin/paclitaxel nanoparticle for enhanced synergistic antitumor efficacy, Colloids Surfaces B Biointerfaces 128 (2015) 419–426.
[17] Z. Yang, N. Sun, R. Cheng, C. Zhao, Z. Liu, X. Li, J. Liu, Z. Tian, pH multistage responsive micellar system with charge-switch and PEG layer detachment for co-delivery of paclitaxel and curcumin to synergistically eliminate breast cancer stem cells, Biomaterials 147 (2017) 53–67.
[18] W. Wei, Y. Sun, M. Zhu, X. Liu, P. Sun, F. Wang, Q. Gui, W. Meng, Y. Cao, J. Zhao, Structural insights and the surprisingly low mechanical stability of the Au-S bond in the gold-specific protei GolB, J. Am. Chem. Soc. 137 (2015) 15358–15361.
[19] A. Jain, K. Cheng, The principles and applications of avidin-based nanoparticles in drug delivery and diagnosis, J. Contr. Release 245 (2017) 27–40.
[20] S. Maiti, P. Paira, Biotin conjugated organic molecules and proteins for cancer therapy: a review, Eur. J. Med. Chem. 145 (2018) 206–223.
[21] Y. Singh, K. Viswanadham, A.K. Jajoriya, J.G. Meher, K. Raval, S. Jaiswal, J. Dewangan, H.K. Bora, S.K. Rath, J. Lal, D.P. Mishra, M.K. Chourasia, Click biotinylation of PLGA template for biotin receptor oriented delivery of doxorubicin hydrochloride in 4T1 cell-induced breast cancer, Mol. Pharm. 14 (2017) 2749–2765.
[22] W.H. Chen, X.D. Xu, H.Z. Jia, Q. Lei, G.F. Luo, S.X. Cheng, R.X. Zhuo, X.Z. Zhang, Therapeutic nanomedicine based on dual-intelligent functionalized gold nanoparticles for cancer imaging and therapy in vivo, Biomaterials 34 (2013) 8798–8807.
[23] Y. Ding, Y.Y. Zhou, H. Chen, D.D. Geng, D.Y. Wu, J. Hong, W.B. Shen, T.J. Hang, C. Zhang, The performance of thiol-terminated PEG-paclitaxel-conjugated gold nanoparticles, Biomaterials 34 (2013) 10217–10227.
[24] L. Li, Nafiujjaman Nurunnabi, Y.K. Lee, K.M. Huh, GSH-mediated photoactivity of pheophorbide a-conjugated heparin/gold nanoparticle for photodynamic therapy, J. Control. Release 171 (2013) 241–250.
[25] X. Wang, X. Cai, J. Hu, N. Shao, F. Wang, Q. Zhang, J. Xiao, Y. Cheng, Glutathione-triggered “off-on” release of anticancer drugs from dendrimer-encapsulated gold nanoparticles, J. Am. Chem. Soc. 135 (2013) 9805–9810.
[26] I.R. Fernando, D.P. Ferris, M. Frasconi, D. Malin, E. Strekalova, M.D. Yilmaz, M.W. Ambrogio, M.M. Algaradah, M.P. Hong, X. Chen, M.S. Nassar, Y.Y. Botros, V.L. Cryns, J.F. Stoddart, Esterase- and pH-responsive poly(β-amino ester)-capped mesoporous silica nanoparticles for drug delivery, Nanoscale 7 (2015) 7178–7183.
[27] M. Hu, P. Huang, Y. Wang, Y. Su, L. Zhou, X. Zhu, D. Yan, Synergistic combination chemotherapy of camptothecin and floxuridine through self-assembly of amphiphilic drug–drug conjugate, Bioconjug. Chem. 26 (2015) 2497–2506.
[28] T. Zhang, P. Huang, L. Shi, Y. Su, L. Zhou, X. Zhu, D. Yan, Self-assembled nanoparticles of amphiphilic twin drug from floxuridine and bendamustine for cancer therapy, Mol. Pharm. 12 (2015) 2328–2336.
[29] X. Liu, Q. Huang, C.X. Yang, Q.Z. Zhang, W. Chen, Y.Q. Shen, M.H. Sui, A multi-stimuli responsive nanoparticulate SN38 prodrug for cancer chemotherapy, J. Mater. Chem. B 5 (2017) 661–670.
[30] H.J. Jung, M. Abou-Jaoude, B.E. Carbia, C. Plummer, A. Chauhan, Glaucoma therapy by extended release of timolol from nanoparticle loaded silicone-hydrogel contact lenses, J. Control. Release 165 (2013) 82–89.
[31] H.J. Jung, A. Chauhan, Temperature sensitive contact lenses for triggered ophthalmic drug delivery, Biomaterials 33 (2012) 2289–2300.
[32] W. Zhang, F. Wang, Y. Wang, J. Wang, Y. Yu, S. Guo, R. Chen, D. Zhou, pH and near-infrared light dual-stimuli responsive drug delivery using DNA-conjugated gold nanorods for effective treatment of multidrug resistant cancer cells, J. Control. Release 232 (2016) 9–19.
[33] T.C. Chou, Theoretical basis, experimental design, and computerized simulation of synergism and antagonism in drug combination studies, Pharmacol. Rev. 58 (2006) 621–681.
[34] Z. Tu, K. Achazi, A. Schulz, R. Mülhaupt, S. Thierbach, E. Rühl, A. Mohsen, H. Rainer, Combination of surface charge and size controls the cellular uptake of functionalized graphene sheets, Adv. Funct. Mater. 27 (2017) 1701837.
[35] G. Dacarro, P. Pallavicini, S.M. Bertani, G. Chirico, L. D'Alfonso, A. Falqui, N. Marchesi, A. Pascale, L. Sironi, A. Taglietti, E. Zuddas, Synthesis of reduced-size gold nanostars and internalization in SH-SY5Y cells, J. Colloid Interface Sci. 505 (2017) 1055–1064.
[36] J.Q. Lin, H. Zhang, V. Morovati, R. Dargazany, PEGylation on mixed monolayer gold nanoparticles: effect of grafting density, chain length, and surface curvature, J. Colloid Interface Sci. 504 (2017) 325–333.
[37] Z. Tu, V. Wycisk, C. Cheng, W. Chen, M. Adeli, R. Haag, Functionalized graphene sheets for intracellular controlled release of therapeutic agents, Nanoscale 9 (2017) 18931–18939.
[38] B.H. Choi, C.G. Kim, Y. Lim, S.Y. Shin, Y.H. Lee, Curcumin down-regulates the multidrug-resistance mdr1b gene by inhibiting the PI3K/Akt/NF kappa B pathway, Cancer Lett. 259 (2008) 111–118.
[39] M.C. Cavaco, C. Pereira, B. Kreutzer, L.F. Gouveia, B. Silva-Lima, A.M. Brito, M. Videira, Evading P-glycoprotein mediated-efflux chemoresistance using solid lipid nanoparticles, Eur. J. Pharm. Biopharm. 110 (2017) 76–84.